Assessment of sea slope statistical models using a detailed micro-facet BRDF and upwelling radiance measurements

V. Ross[1*], D. Dion[2]
[1] AEREX Avionique Inc., [2] DRDC-Valcartier.

ABSTRACT

An attempt is made to evaluate three different models correlating sea slope variance with wind speed, which are a crucial component of the statistical approach to calculating the sea surface BRDF (Bidirectional Reflectance Distribution Function). The models are those of Cox & Munk, Wu and Mermelstein et al. This is done with the help of publicly available upwelling radiance data taken at the COVE rigid costal platform with a scanning spectral photometer at wavelengths around 444 nm, 501 nm, 677 nm and 864 nm for a wide range of azimuth and elevation angles. The three sea slop variance models are compared with variances inferred from the data by inverting a BRDF models that includes facet hiding and shadowing as well as facet projection weighing. The validity of the models is discussed in the context of varying wind speed and direction. Limitations when dealing with near-horizon BRDF modeling using these statistical models are discussed along with potential improvements.

Keywords: sea surface BRDF, slope variance, visible and infrared background modeling, validation

1. INTRODUCTION

Accurate modeling of the roughness of the sea, particularly of the sea slope statistics, has many beneficial implications in remote sensing and detection applications. Most interactions of radiation with the air-sea boundary depend on the roughness of the interface, more precisely its bidirectional reflectance distribution function (BRDF), and remote measurements of any quantity at or across this boundary will most likely be influenced by it. Because of this, many efforts have been spent on the creation of various types of sea BRDF models. Some involve analytical approximation[1,2,3], while others are based on complex 3D Monte-Carlo surface modeling[4-7] No matter how complex or realistic a model may be, most are firmly based on an understanding of the sea surface slope statistics. This implies that no such model will ever be more accurate than its underlying statistical description of the sea surface. It is therefore of prime importance to possess a model that describes the statistical properties of the sea surface under varying environmental conditions.

One method used to obtain a description of the sea surface statistics is to derive sea slope variances from wave power spectral density spectrum[1,8-10]. Although wave spectrum measurements are relatively easy to obtain, derived slope variances do not always agree with in situ optical measurements or have a limited validity range[8]. It is also possible to try to reproduce natural conditions in a laboratory, but experience has shown that wave tank measurements do not always reproduce field measurements correctly[11]. Direct measurements of sea slope statistics under a wide range of environmental conditions are therefore essential, but campaigns to obtain these have historically been few and far apart. The lack of published results is mostly due to the experimental difficulties involved. Regardless of these shortcomings, a few models have emerged from these methods, but validations of these are sparse.

The objective of this paper is to add to the validation of three of the most widely used sea slope variance models. To do this, a detailed BRDF model is inverted to extract slope probability density values from sun glint radiance measurements under varying meteorological conditions. Slope probability density functions (PDF) are then fitted to the extracted values with slope variances left as free parameters. We then verify how the sea slope variances obtained in this way compare with the values predicted by the models.

[*] vincent.ross.AEREX@drdc-rddc.gc.ca; phone: 1 418 844-4000 ext: 4728; fax: 1 418 844-4511

The data used in this study is publicly available from the CERES Ocean Validation Experiment (COVE). We used all data taken on clear days in the months of November 2003 trough January 2004 (November 2 and 3, December 26, 27, 28 and 31 and January 7 and 11). The data is measured from a rigid ocean platform located 25 km off the cost of Virginia Beach at the mouth of Chesapeake Bay. The instrument is a SP1A Schultz spectral photometer that scans the sea surface at 10 elevation angles from 2^o to 72^o from the horizon. For each elevation angles, it scans about 180^o of azimuth at 2.5^o intervals. For each new scan, filters are rotated between 444 nm, 501 nm, 677 nm and 864 nm. More information on the instrument and data can be found in Su et al. (2002)[12]. Note that the scanning resolution and spans have slightly been modified since their publication. Meteorological and environmental data for the COVE site is also readily available from the NASA Langley CERES ARM Validation Experiment (CAVE)[13,14].

2. SLOPE VARIANCE MODELS

The first complete set of sea slope statistical measurements was obtained by Cox and Munk in 1954 from photographs of sun glint[15,16]. The photographs were taken from an airplane at about 600 m in altitude while meteorological data was gathered from a ship down below. Care was taken for the sun to be high enough so that the effects of shadowing and multiple reflections were small. They found that the probability density function (PDF) was well fitted by a Gram-Charlier expansion whose first order term is the Gaussian

$$p_0(\zeta_x,\zeta_y,U)\approx\frac{1}{2\pi\sigma_x\sigma_y}\exp\left\{-\frac{1}{2}\left(\frac{\zeta_x^2}{\sigma_x^2}+\frac{\zeta_y^2}{\sigma_y^2}\right)\right\} \tag{1}$$

where U is the wind speed at 12.5 m (41 ft), ζ_x and ζ_y are the upwind and cross wind slopes, and σ_x^2 and σ_y^2 are the upwind and crosswind variances. They also found a strong linear correlation of the variances with wind speed

$$\begin{aligned}\sigma_x^2&=0.00316U\pm0.004\\ \sigma_y^2&=0.003+0.00192U\pm0.004.\end{aligned} \tag{2}$$

Additional terms are needed to correct for kurtosis (peakedness) and skewness,

$$\begin{aligned}p\approx p_0\Big\{&1-\frac{1}{2}c_{21}\left(Y^2-1\right)X-\frac{1}{6}c_{03}\left(X^3-3X\right)\\&+\frac{1}{24}c_{40}\left(Y^4-6Y^2+3\right)+\frac{1}{4}c_{22}\left(Y^2-1\right)\left(X^2-1\right)\\&+\frac{1}{24}c_{04}\left(X^4-6X^2+3\right)\Big\},\end{aligned} \tag{3}$$

where

$$X=\frac{\zeta_x}{\sigma_x},\quad Y=\frac{\zeta_y}{\sigma_y}.$$

The Cox & Munk skewness expansion coefficients in equation (3) are given by

$$c_{21}=0.01-0.0086U,\quad c_{03}=0.04-0.033U \tag{4}$$

while the kurtosis coefficients are

$$c_{40}=0.40,\quad c_{22}=0.12,\quad c_{04}=0.23\,. \tag{5}$$

Although the Gram-Charlier series representation of the sea slope PDF has rarely been disputed in the literature (Liu et al.[17] and Plant[18] are a few exceptions), some improvements or alternatives to the slope variance model (2) have been proposed. Two decades after Cox and Munk, Wu reanalyzed their data to notice that a two branch logarithmic function could yield a better fit[11]. Wu later revised his relationship[19] and finally yielded a correlation of sea slope variances with wind speed given by

$$\begin{aligned} \sigma^2 &= (0.90 + 1.20 \ln U) \times 10^{-2} \qquad U \le 7\ m/s \\ \sigma^2 &= (-8.40 + 6.00 \ln U) \times 10^{-2} \qquad U > 7\ m/s \end{aligned} \tag{6}$$

where wind speed is measured at 10 m instead of 12.5 m and σ^2 is the average upwind and crosswind variance. The upwind and crosswind components are obtained from the constant relation $\sigma_y^2/\sigma_x^2 = 0.8$. According to Wu, the two-branches of the equation corresponds to gravity-dominant and capillary-dominant wave regimes respectively.

Since, the advent of the laser has prompted a few other sea slope measurement campaings[20-24]. Results obtained were most of the time in accord with those obtained by Cox and Munk, but occasionally, major deviations were observed. Authors have attempted to correlate these deviations with other environmental parameters such as atmospheric stability or swell conditions. Hwang and Shemdin[23] found that although the state of development of swells had some influence, it was small compared to the effect of atmospheric stability. This was later confirmed by Shaw and Churnside[24] who added their data to that of Hwang and Shemdin and obtained an expression modifying Cox and Munk's variances to take into account atmospheric stability.

Apart from expressions derived from to the original work of Cox and Munk, the only other available relationships are those derived from wave power spectral density spectrum. One such example is the model of Mermelstein et al.[1] in which the Donelan and Pierson wave spectrum[9] is used to extract slope variances. From these variances, they obtain the fitted relations

$$\begin{aligned} \sigma_x &= 0.091 + 0.019U - 4.6 \times 10^{-4} U^2 \\ \sigma_y &= 0.059 + 0.021U - 5.6 \times 10^{-4} U^2 \end{aligned} \tag{7}$$

correlating slope RMS with wind speed.

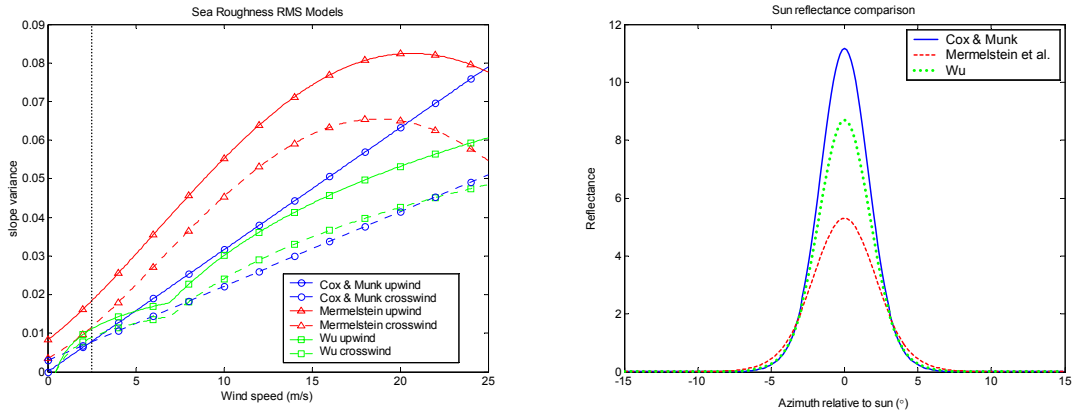

Figure 1: Slope variance variation with wind speed for different models (left) and the resulting upwind sun reflectance for a wind speed of 2.5 ms^{-1}, sun elevation of 10^o and scanning elevation of 10^o below the horizon (right).

All three sea slope variance models (2), (6) and (7) are plotted on the left-hand side of Figure 1. Depending on the wind speed, significant discrepancies exist between the models, especially for low winds. The result in using one model over another to calculate the sun reflectance is shown on the right pane of Figure 1 for a wind speed of 2.5 ms^{-1} (vertical dotted line in the left pane). The differences in reflectance are considerable, and will be of similar amplitude independently of the BRDF model chosen for the calculation. Furthermore, the variation of variances due to atmospheric stability not accounted for in this calculation is reported by Shaw and Churnside[24] to potentially exceed a factor of two. One can thus appreciate the sensitivity of the variance model in the calculation of the BRDF.

3. METHOD

The method used to compare and validate the sea slope variance models consists in four steps. The first is to subtract the parasitic effects from the solar glint measurements. This mainly includes sky radiance, subsurface scattered radiance, path radiance and transmittance. The second step is to put down a model that describes as many physical aspects of the sea surface BRDF as possible. Then, using this model, probability density values can be extracted from measured radiance results. This is very similar to the method used by Cox & Munk[15,16], except that present day computational methods permit us to use a more detailed BRDF, which leads to fewer constraints on the geometrical validity. Finally, in the last step of the method, a PDF representation such as the Gram-Charlier expansion is fitted to the probability density points so that its variance can be correlated with environmental conditions.

The micro facet BRDF approach assimilates a small region of the surface to a flat facet whose slope components are governed by a PDF. The radiance reflected by a particular facet is simply the product of the Fresnel reflected radiance with the probability of the facet being oriented in the proper direction for the reflection to reach the receiver. The basis in calculating the radiance reflected from an extended source by a rough surface such as the sea is then given by

$$L_r\left(\phi_r,\theta_r,\phi_s,\theta_s,U\right) = L_i \iint_{source} r(\zeta_x,\zeta_y)q(\zeta_x,\zeta_y,U)d\zeta_x d\zeta_y, \tag{8}$$

where L_i is the incident radiance of the source, given that it is constant on its entire surface, $r(\zeta_x,\zeta_y)$ is the Fresnel reflectance of the facet with slopes (ζ_x,ζ_y) and $q(\zeta_x,\zeta_y,U)$ is the modified PDF which include effects such as shadowing, etc. The integration is done on all slopes that can reflect a point on the source with center coordinates $(\phi_s,\ \theta_s)$ from the facet towards the receiver located at $(\phi_r,\ \theta_r)$ with the facet as the reference. The coordinate system and other quantities relevant to the problem are illustrated in Figure 2. Since q is a PDF, it must be normalized to unity

$$\int_{-\infty}^{\infty}\int_{-\infty}^{\infty} q(\zeta_x,\zeta_y,U)d\zeta_x d\zeta_y = 1. \tag{9}$$

The expression for q is rather complex and a full description of its components is out of the scope of this paper. A brief description of it will be presented here while more details can be found in the cited references. A good approximation for the modified PDF that accounts for shadowing of wave facets by other waves, hiding of facets from the receiver and projection weighing of the facets according to there orientation is given by

$$q(\zeta_x,\zeta_y) = \left\{\frac{1+\Lambda(v_r)}{1+\Lambda(v_r)+\Lambda(v_s)}\right\}\frac{p(\zeta_x,\zeta_y)W(\zeta_x,\zeta_y)H_{\zeta}(\zeta_x,\zeta_y)}{\int_{-\infty}^{\infty}\int_{-\infty}^{\infty} p(\zeta_x,\zeta_y)W(\zeta_x,\zeta_y)H_{\zeta}(\zeta_x,\zeta_y)d\zeta_x d\zeta_y}, \tag{10}$$

where all dependencies on wind speed are implicit for conciseness and (ζ_x,ζ_y) is calculated from the receiver and source position. Note that in the following description, as it is done here, hiding functions always refer to the fraction of facets

that can be seen by the receiver while shadowing functions represents the fraction of facets that can be illuminated by the source. In equation (10),

$$H_{\varsigma}(\zeta_x, \zeta_y) = \Upsilon(\mathbf{U}_n \cdot \mathbf{U}_r) \tag{11}$$

where Υ is the Heaviside function and is defined as

$$\Upsilon(x) = \begin{cases} 0 & , \quad x \le 0 \\ 1 & , \quad x > 0. \end{cases} \tag{12}$$

This hiding function accounts for the fact that the backsides of the waves are not visible from the receiver. Since different facets are tilted differently with respect to the receiver, they must be weighed accordingly. The projection weighing function has been shown by Zeisse[2,3] to be

$$\begin{aligned} W(\zeta_x, \zeta_y) &= \frac{\cos\omega}{\cos\theta_n} \\ &= \frac{\mathbf{U}_n \cdot \mathbf{U}_r}{z_n}. \end{aligned} \tag{13}$$

Finally, the expression in curly braces is the result of integrating the azimuthally varying Smith[25,26] hiding function

$$\begin{aligned} H_w(\theta_r, \phi_r, h) &= \left[1 - \frac{1}{2}\operatorname{erfc}(h)\right]^{\Lambda(v_r)} \\ \Lambda(v_r) &= \frac{\exp(-v_r^{\,2}) - v_r\sqrt{\pi}\,\operatorname{erfc}(v_r)}{2v_r\sqrt{\pi}} \quad , \quad v_r = \frac{\cot(\theta_r)}{\sqrt{2}\sigma(\phi_r)} \\ \sigma^2(\phi_r) &= \frac{\sigma_x^{\,2} + \sigma_y^{\,2}}{2} + \frac{\sigma_x^{\,2} - \sigma_y^{\,2}}{2}\cos(2\phi_r) \end{aligned} \tag{14}$$

and the equivalent shadowing function (obtained by replacing subscripts *r* by *s*) over a Gaussian facet height PDF in the range [-∞,∞], and normalizing according to (9). Smith hiding and shadowing functions account for the hiding or shadowing of a facet of height *h* by other waves. The integral at the denominator of (10) is the result of normalizing *q* according to (9) for the remaining hiding functions. This is necessary because hiding and weighing functions take facets out of *q* so that it would no longer be normalized to unity.

Using an approximation found in Cox and Munk[15], and further pointed out by Zeisse[2,3], the integral over the sun's disk can be approximated and the full expression for (8) becomes

$$L_r(\theta_r, \phi_r, \theta_s, \phi_s, U) \simeq L_i \frac{\pi\varepsilon^2 r(\zeta_x, \zeta_y) q(\zeta_x, \zeta_y, U)}{4 z_n^{\,3} (\mathbf{U}_n \cdot \mathbf{U}_r)}. \tag{15}$$

where ε is the sun's angular radius.

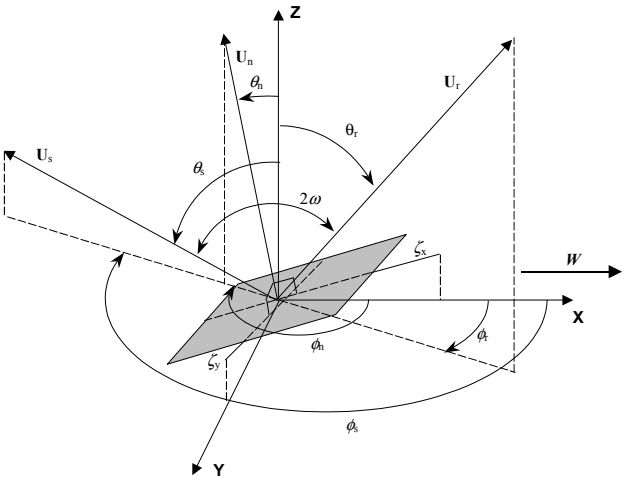

Figure 2: Coordinate system and relevant quantities representation. Subscript *r* refers to the receiver, *s* to the source and *n* to the facet normal.

Calculating L_i and measuring L_r, q can be found and p numerically extracted from it. An approximation is necessary though, since the Smith functions (14) also depend on the slope variances. These are approximated by using the Cox and Munk slope variances (2). Fear that this could bias the results towards the Cox and Munk statistics should be put aside for many reasons. First of all, shadowing is a very small component of the BRDF and along with multiple reflections should not account for more than 2 or 3 percent of the overall reflectance when the wind is blowing at 10 ms^{-1} and the sun is 10^o over the horizon[27]. Furthermore, the shadowing functions are not nearly as sensitive to variations in slope variance as is the PDF. Finally, the shadowing functions are mainly multiplicative factors over large sea surface areas and should have a very minor impact on the extracted variances. , should there be a bias, it would likely be much smaller the measurement errors.

The subtraction of parasitic radiance from the data presented somewhat of a problem, since the radiance measurements that were available to us had not yet been calibrated. In the most of the analysis, uncalibrated data is not a problem since the variance of a nearly Gaussian PDF does not depend on its amplitude. In order to find the approximate calibration constants we took advantage of the property in equation (9). An iterative procedure was set up so that modeled sky and diffuse radiance were subtracted from the data, the PDF was extracted from the result in the way described previously, and calibration constants were adjusted until the PDF normalized to unity. The sun irradiance is available from measurements taken at COVE, while sky radiances, detector to surface path radiances and transmittances are calculated using MODTRAN 4.0[28,29] with atmospheric profiles and aerosol optical properties modeled with IRBLEM[30]. Radiance calculations are done with the two stream multiple scattering approximation. This approximation may cause some inaccuracies, but is necessary for speed since sky radiances are calculated at 3^o increments in azimuth and elevation. A chlorophyll concentration value of about 3 mg/m^3 for the period was obtained from the SeaWiFS satellite, and the subsurface scattering by water and phytoplankton was approximated[31,32]. Calibration constants were calculated for an arbitrary subset of the available data (31^{st} of December) and then used in the entire analysis. We do not expect these calibration constants to be more accurate than about 10% to 20%. Although this might seem somewhat inaccurate, one has to remember that Cox and Munk pointed out that the background is very faint when compared to the sun glint, especially when red filters are used. We then expect the parasitic radiance subtraction to be less of a problem when using the 677 nm and 864 nm filtered data and greater uncertainties to be constrained to very steep slopes (wings of the distribution).

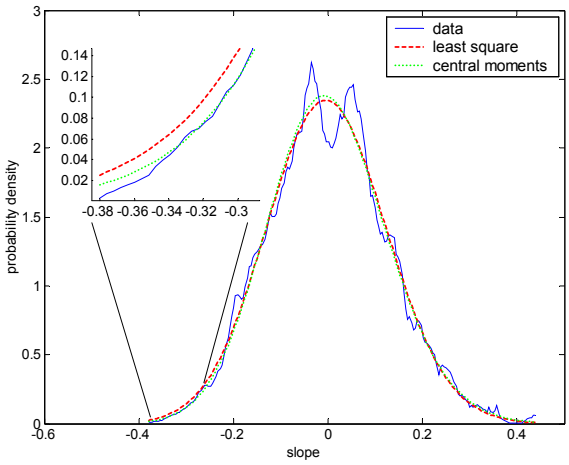

Figure 3: Typical example of integrated PDF data fitted with a Gram-Charlier distribution by methods of least squares and central moments.

Once the PDF values have been extracted, they are interpolated to a fixed slope grid and integrated in both upwind and cross wind directions yielding the measured components of the PDF. Finally, a Gram-Charlier is fitted to these components using two different methods. The first is a simple least-square fit while the second is done by computing the central moments of the distribution. Both methods yield slightly different values, but these differences are not systematic. We thus consider the average of the two in order to reduce errors. A typical example of fitted PDFs is provided in Figure 3. It is obvious that both methods yield similar results, although the central moments may better reproduce low slope values (better kurtosis) as seen in the blown up part of the curve.

4. RESULTS AND DISCUSSION

All the extracted data for any given day was binned in wind speed increments so that each variance point was calculated from about the same number of PDF points. Since each instrument scan is composed of nearly instantaneous measurements, they are extremely noisy, and since each scan takes about 4.5 minutes, the data must be averaged over very long periods in order to lower the noise to acceptable levels. Typically, the data is averaged over 3h. Because of this, there can be large variances in wind speed for each point, sometimes reaching 25%. The uncertainties on the slope variance stemming from the fitting procedure are usually smaller, although there are very large uncertainty differences from one slope variance point to another. Errors are especially large for low winds since the sun glint is much noisier and constrained to smaller regions of the scans.

The resulting slope variances are plotted in Figure 4 along with the three models that we wish to assess in both upwind and crosswind components. Although an increase in slope variance with wind speed is clearly visible, the data is somewhat scattered. This is not surprising when considering the fact that our data is taken with a large array of stability conditions from very stable to very unstable over the sea surface. According to Shaw and Churnside[12], such variations, especially under unstable conditions, can account for changing the slope variance values by a factor of more than 2.0.

Nevertheless, we note from Figure 4 that the Mermelstein model overestimates just about all data points. We thus decided to rule it out from the rest of our analysis. However, the Cox and Munk as well as the Wu models seem to follow a very similar trend to our data. By simple inspection, it is hard though to verify which model provides better fit. This was expectable since they both originate from the Cox and Munk data set. In order to estimate which represents a better fit to our data, weighed residuals are calculated and presented in Table 1. The weighs are calculated from the standard error (σ_s) of each fit of the PDF data to Gram-Charlier distributions as $w = 1/\sigma_s^2$. From Table 1 it seems that the simple linear fit found by Cox and Munk is in better agreement with our data in both >7 ms^{-1} and <7 ms^{-1} wind speed ranges. The better fit originally obtained by Wu with the Cox and Munk data might simply have been the result of

adding a degree of freedom to the empirical equations. In any case, because of the disperse nature of slope variance data, much more points would be needed to obtain an empirical formulation differing from linear with enough confidence.

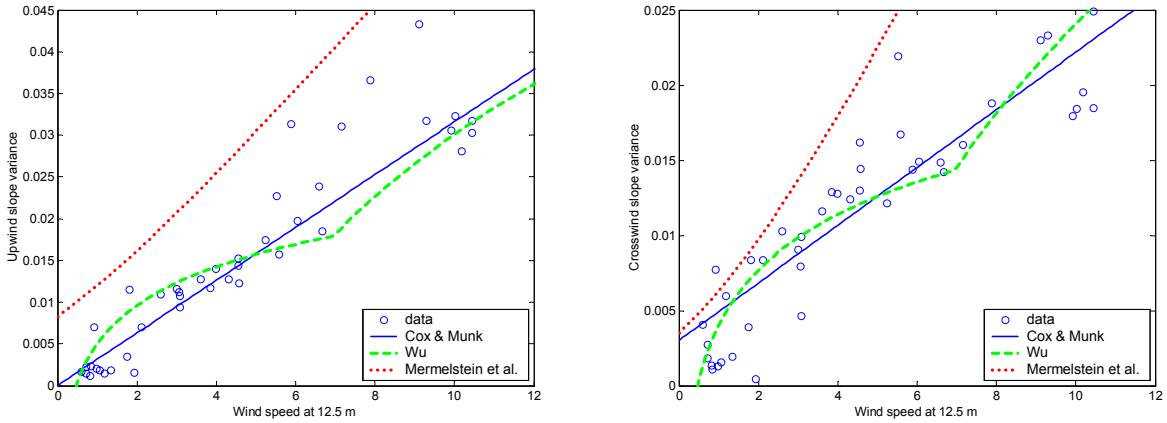

Figure 4: Our data plotted along with all three variance models in the upwind (left) and crosswind (right) components.

Table 1: Weighed residuals between data and models

	Upwind < 7 ms^{-1}	Upwind > 7 ms^{-1}	Crosswind < 7 ms^{-1}	Crosswind > 7 ms^{-1}
Cox & Munk	0.0503	0.1324	0.0255	0.0190
Wu	0.0810	0.2386	0.0249	0.0593

The fact that our data spans not only environmental conditions, but also many different geometrical configurations (sun and receiver elevation) permits us to evaluate the possible influence of these on the statistics. In order to do this, the same procedure as described in the above sections was applied to subsets of the data with different receiver elevations. Since this reduces dramatically the number of PDF data points in each subset, only the least square method was used since it gives better results when the PDF is truncated in slope. Furthermore, since the sun glint region tends to move towards the horizon, very few points exist passed 30^o in elevation. Finally, to reduce the noise further, only wide wind speed intervals are considered.

Figure 5 gives the result of applying this procedure to different wind speed intervals: 0 to 4 ms^{-1} (squares), 7 to 12 ms^{-1} (triangles) and the total average from 0 to 12 ms^{-1} (circles). The results correspond to the average of the upwind and crosswind components since the amplitude of the effect is the same in both axes of the PDF. There seems to be a rapid spike in sea slope variance as the receiver peers closer to the horizon. One must be very careful in interpreting these results though. This is because the solar glint region tends to move closer to the horizon as the wind speed increases. Consequently, results obtained closer to the horizon might be biased towards higher wind speeds en hence higher variances. This bias is nonetheless an important result, since we might need to consider it when integrating radiance near the horizon for long time periods, or even for shorter periods when the wind is very gusty.

To verify if this bias is the only cause of the increase in slope variance towards the horizon, we repeated the procedure with much smaller wind bins (only 1 ms^{-1}) and averaged the very noisy results into one single curve. When comparing the result (dotted curve) to the 0 to 12 ms^{-1} curve obtained previously, we immediately notice that a bias was in fact removed. However, there still remains a very sharp increase of about 30% in variance close to the horizon. To explain this, one must first understand that most BRDF models (ours inclusively) consider the slope variances to be uncorrelated with height. This means that the statistics at the troughs and at the crests of waves are the same. It must also

be pointed out that as we peer towards the horizon, the bottom of waves become more and more hidden by other waves until we only see the very top of the highest waves. The hypothesis of uncorrelated height and slope statistics might in fact be false. Many authors such as Longuet-Higgins[33], Phillips[34] and Liu[8,17] agree that the departure of the sea slope PDF from Gaussian might be the consequence of sharp crests and shallow troughs. If this is true, what we observe could simply result from measuring more statistics from the crests closer to the horizon. Although correlated statistics add much complexity to BRDF calculations, results such as those shown here may lead to empirical solutions, where the effect is incorporated into the slope variance relationships. In such a case, the slope variances would also depend on the source and receiver geometry.

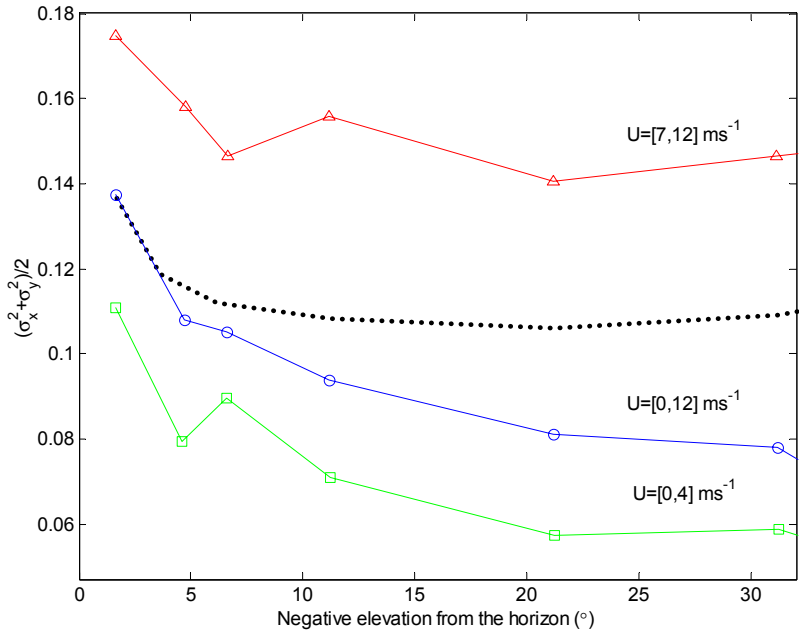

Figure 5: Observed correlation of average sea slope variances with angle of elevation

5. CONCLUSION

By numerically inverting a detailed BRDF model, we were able to obtain a new set of sea slope variance data from sea glint radiance measurements. Our method allows one to obtain sea slope statistics with relative ease, even if the data are not calibrated in radiance. Even though it is most likely less accurate than modern laser scanning techniques, the much-increased ease in instrument setup and data processing could eventually compensate by facilitating the acquisition of large quantities of data.

We compared models of Cox and Munk, Wu and Mermelstein et al. with slope variances derived from COVE measurements made from November 2003 trough January 2004. It was found that the model from Mermelstein et al. strongly overestimates the slope variances when compared to our measurements. Furthermore, the model of Cox and Munk and that of Wu compare well with our data, although the Cox and Munk model seems slightly closer to our measurments.

The effect of look angle on the sea slope variance was also assessed. It was found that a bias exists that increases the slope variance by about 30% near the horizon. This can be explained by two distinct causes. First, under variable wind conditions, statistics closer to the horizon will be biased towards the results for higher winds since they tend to move the sun glint region in the direction of the horizon. The second cause for the bias may come from the combined facts that crests of waves have higher slope variances than their troughs, and that we see less of the troughs as we look closer to the horizon.

The method used in this study will hopefully permit us to gather larger amounts of statistical data concerning sea slopes. Once we have enough data, trends correlating slope statistics with environmental and geometrical parameters will become easier to find, something that most BRDF models could greatly benefit from. This process might even become much simpler by current work by our group to obtain a good analytical approximation to the BRDF expression. Because of this, it should eventually be possible to quickly obtain PDF values from sun glint measurements analytically.

6. ACKNOWLEDGMENTS

The authors would like to give many thanks to Ken Rutledge for his valuable help in obtaining the COVE data and in understanding it and the instrument. Thanks also to David Rutan for promptly making available to us the meteorological data from the COVE site. Finally, we are in great depth to the entire team responsible for the SP1A instrument at COVE for making its data public.

REFERENCES

1. Mermelstein M.D., Shettle E.P., Takken E.H. and Priest R.G., "Infrared radiance and solar glint at the ocean-sky horizon", *Appl. Opt.*, **33** (25), 6022-6034, 1994.
2. Zeisse, C. R. "Radiance of the Ocean Horizon", *NCCOSC RDT&E TR-1660.*, Naval Command, Control and Ocean Surveillance Center, RDT&E Division, San Diego, CA., 1994.
3. Zeisse, C. R. "Radiance of the Ocean Horizon", *J. Opt. Soc. Am.* **12**, 2022-2030 1995
4. R. W. Preisendorfer and C. D. Mobley, Albedos and glitter patterns of a wind-roughened sea surface, *J. Phys. Oceanogr.* 16, 1293-1316, 1986.
5. Bourlier, C., Saillard J., and Berginc G., "Effect of correlation between shadowing and shadowed points on the Wagner and Smith monostatic one-dimensional shadowing function," *IEEE Trans. Ant. Prop.*, **48**, 437–446, 2000.
6. Bourlier, C. and Berginc G., "Microwave analytical backscattering models from randomly rough anisotropic sea surface—comparison with experimental data in c and ku bands", *PIER*, **37**, 31–78, 2002.
7. Henderson B., Theiler J. and Villeneuve P. V., "The polarized emissivity of a wind-roughened sea surface: a Monte-Carlo model" *Rem. Sens.of Env.* **88**, 453-467, 2003.
8. Liu Y., M.-Y. Su M.-Y., Yan X.-H. and Liu W. T., "The mean-square slope of ocean surface waves and its effects on radar backscatter", *J. Atmos. Oceanic Tech.,* **17,** 1092-1105, 2000.
9. Donelan M. A. and Pierson W. J., "Radar scattering and equilibrium range in wind-generated waves with application to scatterometry", *J. Geophys. Res.,* **92,** 4971-5029, 1987.
10. Apel J. R., "An improved model of the ocean surface wave vector spectrum and its effects on radar backscatter", *J. Geophys. Res.,* **99,** 16 269-16 291, 1994.
11. Wu J., "Mean squared slopes of the wind-disturbed water surface, their magnitude, directionality, and composition", *Radio Science*, **25,** 37-48, 1990.
12. Su W., Charlock T.P., Rutledge K., "Observations of Reflectance Distribution Around Sunglint from a Coastal Ocean Platform", *Appl. Opt.*, **41** (35), 7369-7383, 2002.
13. Rutan, D.A., Rose F.G., Smith N.M, Charlock T.P., "Validation data set for CERES surface and atmospheric radiation budget (SARB)", *WCRP/GEWEX Newsletter*, **11** (1), 11-12, 2001.
14. Jin Z., Charlock T.P., Rutledge K., "Analysis of Broadband Solar Radiation and Albedo over the Ocean Surface at COVE", *J. Atmos. & Ocean Tech.,* **19**, 1585-1601, 2002.
15. Cox C. and Munk W., "Measurement of the roughness of the sea surface from photographs of the sun glitter", *J. Opt. Soc. Am.* **44**, 838-850, 1954.
16. C. Cox and W. Munk, "Statistics of the sea surface derived from sun glitter", *J. Mar. Res.* **13**, 198-227, 1954.
17. Liu Y., Yan X.-H. and Hwang, P. A. "The probability density function of the ocean surface slopes and its effects on radar backscatter", *J. Phys. Oceanogr.,* **27,** 782-797, 1997.
18. Plant, W. J., A new interpretation of sea-surface slope probability density functions, *J. Geophys. Res.*, **108** (C9), 3295-3298, 2003.
19. Wu J., "Sea-surface slope and equilibrium wind-wave spectra", *Phys. Fluids* , **13**, 741-747, 1972.
20. Hughes B. A., Grant H. L. and Chappell R. W., "A fast response surface-wave slope meter and measured wind-wave moments", *Deep-Sea Res.* **24,** 1211-1223, 1977.

21. Tang S., and Shemdin O. H., "Measurement of high frequency waves using a wave follower", *J. Geophys. Res.,* **88** (C14), 9832-9840, 1983.
22. Haimbach S. P. and Wu J., "Field trials of an optical scanner for studying sea-surface fine structures", *IEEE J. Ocean. Eng.*, **OE-10** (4), 451-453, 1985.
23. Hwang, P. A. and Shemdin O. H., "The dependence of sea surface slope on atmospheric stability and swell conditions", *J. Geophys. Res.,* **93** (C11), 13903-13912, 1988.
24. Shaw J. A. and Churnside J. H., "Scanning-laser glint measurements of sea-surface slope statistics", *Appl. Opt.*, **36**, 4202-4213, 1997.
25. Smith, B. G., "Lunar surface roughness, shadowing and thermal emission", *J. Geophysical Research*, **72**, (16), 4059–4067, 1967.
26. Smith, B. G., "Geometrical shadowing of a random rough surface," *IEEE Trans. Ant. Prop.*, **15**, 668–671, 1967
27. R. W. Preisendorfer and C. D. Mobley, Albedos and glitter patterns of a wind-roughened sea surface, J. Phys. Oceanogr. 16, 1293-1316, 1986.
28. Berk, A., Bernstein L.S., and Robertson D. C., "MODTRAN: A Moderate Resolution Model for LOWTRAN7", Rep. GL-TR-89-0122, *Air-Force Geophysics Lab.*, Bedford, MA, 1989.
29. Acharya P.K., Berk A., Anderson G.P., Larsen N.F., Tsay S-Chee, and Stamnes K.H., "MODTRAN4: Multiple Scattering and Bi-Directional Reflectance Distribution Function (BRDF) Upgrades to MODTRAN", *Proc. of SPIE, Optical Spectroscopy Techniques and Instrumentation for Atmospheric and Space Research,* **3756,** 19-21, July 1999.
30. D. Dion, L. Gardenal, L. Forand, M. Duffy, G. Potvin and S. Daigle, "IR Boundary Layer Effects Model (IRBLEM) ", IRBLEM software documentation, January 2003.
31. Gordon H. R., Brown O. B., Evans R. H., Brown J. W., Smith R. C., Baker K. S. and Clark D. K., "A semianalytic radiance model of ocean color," *J. Geophys. Res.,* **93,** 10 909–10 924, 1988.
32. Morel A. and Gentili, "Diffuse reflectance of oceanic waters: bidirectional aspects", *Appl.Opt.,* **32,** 6864-6879, 1993.
33. Longuet-Higgins, M. S., "The generation of capillary gravity waves by steep gravity waves", *J. Fluid Mech.,* **16,** 138-159, 1963.
34. Phillips, O. M., "The dynamics of the upper Ocean" 2nd ed. Cambridge University Press, 336 pp.